de Haas-van Alphen Effect in Palladium*

L. R. Windmiller, J. B. Ketterson, and S. Hörnfeldt†
Argonne National Laboratory, Argonne, Illinois 60439
(Received 14 January 1971)

Measurements of the de Haas–van Alphen (dHvA) extremal areas for the magnetic field in seven nonsymmetry crystallographic planes have been performed in Pd. All three sheets of the Fermi surface expected from band-structure calculations were observed, and the agreement between the calculated and observed surfaces is satisfactory. The shapes of the surfaces are, on the whole, very similar to those in Pt. An area-to-radii inversion has been accomplished for the Γ-centered electron surface and the number of carriers was determined by numerical integration. Effective-mass measurements were performed in four nonsymmetry crystallographic planes. The anisotropy of the observed effective masses for the Γ-centered surface is radically different from Pt, thus showing that although the surfaces are quite similar in shape, the underlying band structures (velocities) are quite different. Effective masses determined from band-structure calculations are shown to be consistent with the experimental values if renormalization effects are taken into account. Masses on the heavy open-hole surface are found to be more enhanced than those on the Γ-centered surface. Spin-splitting zeros are observed for all three sheets of the surface. Assuming that the g factor approximates its free-space value of 2.0, we can determine precise values of the g factor at these spin-splitting zeros by using interpolated effective-mass values. On the whole we find the g factor to be somewhat different from 2.0 and anisotropic. Measurements on 0.1 and 0.05 at.% Co in Pd have revealed the existence of exchange splitting in the energy bands associated with these alloys. This has been confirmed both from the disappearance of the spin-splitting zeros and from the observation of beat waists arising from the area shift between the spin-up and spin-down exchange split bands.

I. INTRODUCTION

Palladium is one of the most interesting of all the $3d$, $4d$, and $5d$ transition metals. This interest centers around the nearly ferromagnetic nature of palladium, clearly demonstrated by experiments in which alloying palladium with a few tenths atomic percent of cobalt or iron produces a spontaneous moment at low temperatures.[1,2] For the case of cobalt alloys, the measured moment per cobalt atom corresponds to as many as nine Bohr magnetons in the very dilute alloys. Since cobalt has two unpaired spins this means that, on the average, approximately seven palladium electrons are aligned for each cobalt electron. That such a strong polarization is possible presents convincing evidence for near or incipient ferromagnetism. The large measured static magnetic susceptibility also demonstrates this point.[3] A simple theory which contains many of the features of metallic ferromagnetism is that due to Stoner.[4] In this theory the susceptibility is given by

$$\chi = \frac{\chi_P}{1 - N(E_F)V_{ex}} \equiv \mu_B^2 S N(E_F) , \qquad (1)$$

where χ_P is the usual Pauli susceptibility, $\chi_P = \mu_B^2 N(E_F)$; $N(E_F)$ is the density of states at the Fermi level, and V_{ex} is an effective (exchange) interaction energy. The factor $S = 1/[1 - N(E_F)V_{ex}]$, called the Stoner enhancement factor, may be as large as 15 in palladium. The (Bloch) criterion for ferromagnetism, $N(E_F)V_{ex} \geq 1$, is thus not quite satisfied in palladium although small changes in the physical parameters may tip the scale in favor of ferromagnetism.

Recently, it was suggested that local fluctuations in the spin density should be present in a system on the verge of the ferromagnetic instability.[5–7] These excitations have been termed paramagnons. This theory explains why superconductivity is absent in the near noble metals (where the electronic density of states is high and thus superconductivity might be expected). The exchange interaction tends to favor the parallel alignment of neighboring spins for times long enough to suppress the formation of the antiparallel Cooper pairs. An interesting prediction of the spin-fluctuation theory is a renormalization of the electronic density of states. The density of states determined in heat-capacity experiments is 54 states/atom Ry.[8] Recently, several band-structure calculations have been performed[9–12] for Pd, and the resulting (unenhanced) density of states is found to be 32 states/atom Ry. Thus an enhancement factor of approximately 1.70 exists in Pd, a portion of which must be assigned to the ordinary electron-phonon interaction. It is not clear at the present time whether the paramagnon enhancement is numerically significant.

Partly because of these interesting many-body effects, as well as the general interest in the cal-

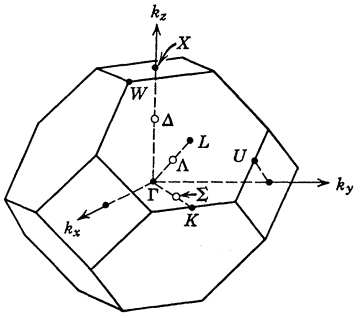

FIG. 1. Brillouin zone for fcc crystal structure.

culation of transition-metal band structures, an exhaustive experimental study of the energy bands of palladium in the immediate vicinity of the Fermi surface using the de Haas–van Alphen (dHvA) effect appears particularly worthwhile. Such a study has recently been completed in Pt (which also has an unusually large susceptibility).[13] Band calculations are, of course, a necessary first step in any future quantitative calculations of the many-body effects. An exhaustive study of a few of the transition metals is necessary to explore the accuracy of the present band-structure calculational techniques. Both the RKKR[14,15] and RAPW[16] (relativistic-augmented-plane-wave) techniques presently rely on approximating the crystal potential by the muffin-tin form and detailed comparisons with accurate experimental Fermi-surface radii should provide a test of the limitations of this form for the potential.

II. BAND STRUCTURE AND FERMI SURFACE OF Pd

The Brillouin zone for the fcc structure is shown in Fig. 1. Two band-structure calculations have been carried out recently on Pd. In the first of these[9,12] an initial APW calculation was performed along the symmetry lines Δ, Z, Q, Λ, Σ, and Σ′. The results of this calculation were then fitted to a combined interpolation scheme[17] with an rms energy error of 0.0048 Ry ($4d^{10}5s^0$). Since relativistic effects are reasonably important the band structure was then modified as follows. The mass-velocity and Darwin terms were neglected as was the p-state spin-orbit interaction. A phenomenological single-parameter d-state spin-orbit interaction was included in the model Hamiltonian matrix.[18] The strength of the spin-orbit parameter as well as various other parameters including the Fermi energy, d bandwidth, overlap and s-d shift were then varied until agreement was obtained between various calculated and measured experimental dHvA data. The resulting band structure is shown in Fig. 2. The horizontal line shows the position of the Fermi level which was determined from an accurate number-of-states histogram and the requirement that the lowest six conduction bands (12 with spins) of palladium hold exactly five electrons (10 with spin). This band structure predicts four sheets to the Fermi surface and we will now discuss these surfaces in the order of increasing number of carriers. The $L5$ band lies just above the Fermi energy and soon drops below E_F as we move away

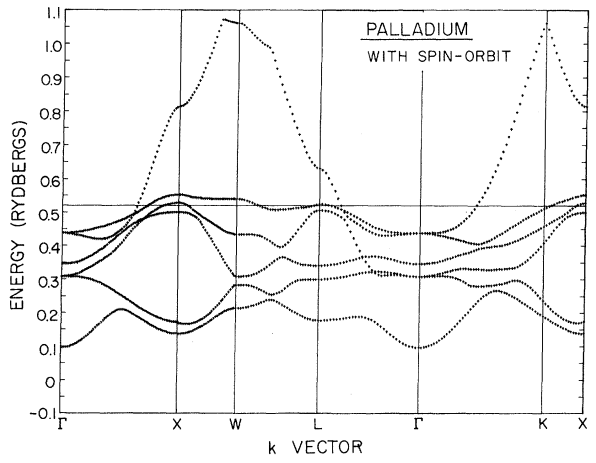

FIG. 2. The band structure of Pd as calculated by Mueller, Freeman, Dimmock, and Furdyna (Ref. 12). The horizontal line shows the Fermi level.

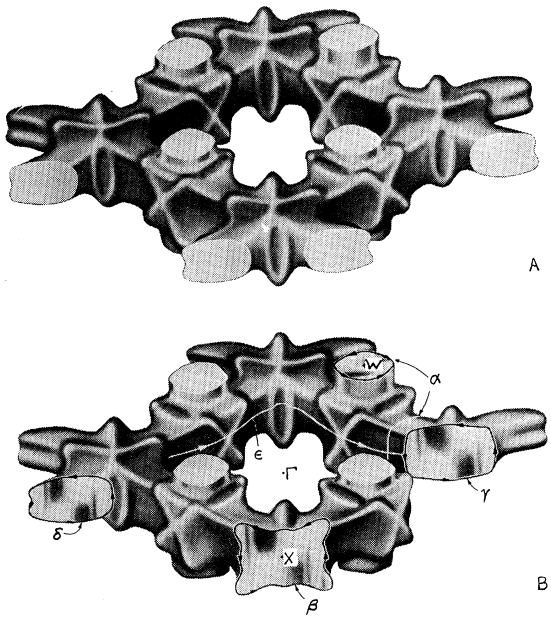

FIG. 3. (a) Open-hole sheet of the Fermi surface of Pd showing connectivity, viewed from approximately the ⟨111⟩ direction. (b) Cutaway of the open-hole sheet of the Fermi surface of Pd showing the various expected extremal orbits.

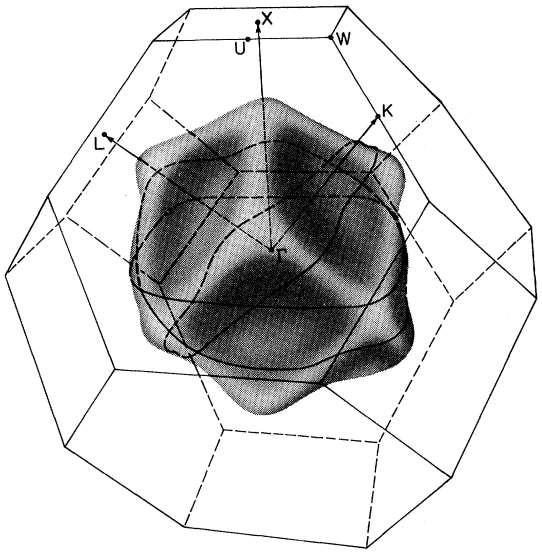

FIG. 4. The Γ-centered electron sheet of the Fermi surface of Pd. Shown are the extremal DHvA orbits for the magnetic field parallel to ⟨100⟩, ⟨110⟩, and ⟨111⟩.

from this point in any direction. Thus, this hole surface is closed and, since it lies near a band extremum, should be nearly ellipsoidal in shape. Since this surface has not been seen in dHvA measurements it is presumed not to exist. A small change in the parameters might conceivably eliminate this surface. A nearly ellipsoidal hole pocket is also associated with the $X4$ level, and this surface is approximately a surface of revolution about the Δ axis. The $X\Gamma$ extension of this surface is approximately 1.56 times larger than XW or XU extensions. We will refer to this surface as the X-centered pocket or simply as the pocket. The dHvA data on this surface are quite complete. The surface containing the next largest number of carriers is that associated with the levels $X5$ and $W5$ both of which lie higher than the Fermi energy. This level passes below the Fermi level in moving from X to Γ or X to U. The hole surface associated with this level is open in the XW or ⟨100⟩ directions and has the connectivity of cylinders extending in the ⟨100⟩ directions which intersect in pairs at the points X of the zone. Figure 3(a) shows this surface. Because of the unusual shape there are several unrelated extremal dHvA orbits which exist for various external magnetic field directions [see Fig. 3(b)]. For the magnetic field parallel to ⟨100⟩ there are two extremal areas, namely, the α and ϵ orbits centered at W and Γ, respectively. For the magnetic field parallel to ⟨110⟩ there are three possible dHvA orbits, namely, the β, γ, and δ orbits of which the first is centered at the point X, and the remaining two do not contain a symmetry point. Of these orbits only the α and γ orbits have been observed in the dHvA experiments. The effective mass of the β (and probably also for the ϵ) orbit is too large to be observed at the lowest temperatures and highest fields available in the present experiment. Detailed calculations for the δ orbit have not been performed so it is not known at present if this orbit exists in palladium, although the orbit has been observed in platinum.[13] The surface containing the largest number of carriers is the electron surface associated with the Γ6 level. Owing to charge neutrality the volume of this surface is equal to the sum of the volumes of all the previously described hole surfaces since the number of holes must equal the number of electrons in an even valent metal such as Pd. This surface is centered at Γ and its extension in the ⟨100⟩, ⟨110⟩, and ⟨111⟩ directions is given by the intersection of the levels Δ6, Σ6, and Λ6 with the Fermi level. The dHvA data for this surface are quite complete. Figure 4 shows the Γ-centered surface along with the extremal orbits for the field parallel to ⟨100⟩, ⟨110⟩, and ⟨111⟩.

The other band-structure calculation[10] which was performed recently has concentrated on the energy range in the immediate vicinity of the Fermi energy; the goal being to obtain accurate first principles (RAPW) values for the electronic density of states $N(E_F)$ as well as the areas and effective masses of the various dHvA orbits. The k vectors on three constant-energy sufaces associated with three values of the energy were calculated in detail and the number of carriers, and the dHvA areas associated with each sheet of the surface calculated by numerical integration. The Fermi energy was then found by interpolating the energy to that value which would give charge neutrality. The density of states and the dHvA quantities were then interpolated to their values at the Fermi energy. Figure 5 shows the (100) and (110) cross sections of the Fermi surface of Pd determined from these calculations.

III. dHvA AND INVERSION THEORY

The detailed theory of the dHvA effect is due to Lifshitz and Kosevich.[19] The oscillatory component to the magnetization associated with the ith extremal cross-sectional area is given approximately by

$$\vec{M} = \hat{M}_i \left(\frac{e}{hc}\right)^{1/2} \frac{A_i \kappa T}{\pi H^{1/2} (\partial^2 A_i / \partial k_H^2)^{1/2}} \times \left(\frac{\exp(-2\pi^2 c\kappa T_x m_i^*/\hbar e H)}{\sinh(2\pi^2 c\kappa T m_i^*/\hbar e H)}\right) \times \sin[2\pi F_i/H + \beta_i] \cos[\pi g_i m_i^*/2m_0] , \quad (2)$$

where the vector direction of the magnetization is given by

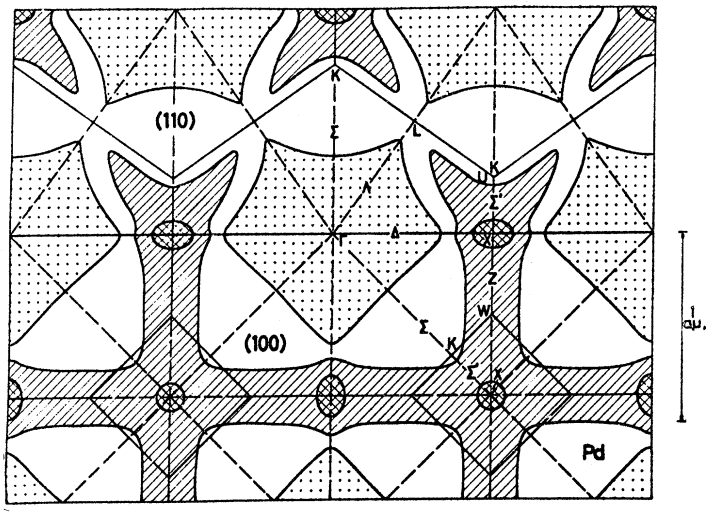

FIG. 5. The (100) and (110) cross sections of the Fermi surface of Pd as calculated by Andersen and Mackintosh (Ref. 10).

$$\hat{M}_i = \hat{H} + \frac{1}{A_i}\frac{\partial A_i}{\partial \theta}\hat{\theta} + \frac{1}{A_i \sin\theta}\frac{\partial A_i}{\partial \varphi}\hat{\varphi} ,$$

and where $F_i = (\hbar c/2\pi e)A_i$ and $m_i^* = (1/2\pi)(\partial A_i/\partial E)$.[20] The extremal areas are determined by observing the frequency of the oscillations in the magnetization as the magnetic field is varied. The effective masses are determined by observing the temperature variation in the amplitude of the oscil-

tion.[29–34] The first technique is applicable for closed sheets of the Fermi surface possessing inversion symmetry. In the case where the radius vector from the inversion center is single-valued, one can expand the angular dependence of the area and radii squared as follows:

$$A(\theta, \varphi) = \sum_{l,m} [\gamma^g_{l,m} C^g_{l,m}(\theta, \varphi) + \gamma^u_{l,m} C^u_{l,m}(\theta, \varphi)] , \quad (3a)$$

determined by interpolating neighboring values of m^*, one can determine the g factor by assuming some value for the integer r.

The quantities measured in a dHvA experiment are all orbital averages of certain more fundamental point properties of the Fermi surface. Using a variety of inversion schemes[21–34] it is possible in certain cases to derive these point properties from measurements of the orbital properties. Two techniques have been employed; one represents the surface in spherical harmonics[22–28] while the other uses a Fourier-series representa-

all 10 crystallographic point groups possessing inversion symmetry.[23,26] For the case of Pd we will be concerned only with the point groups D_{4h} and O_h. The z axis is chosen as the fourfold axis for the D_{4h} group and from this fourfold symmetry it follows that $m = 0 \pmod 4$. Since the z axis lies in a mirror plane we have $\gamma^u_{l,m} = \beta^u_{l,m} = 0$ (with the x axis also in the mirror plane). The full cubic group is more complicated since the existence of more than one fourfold axis introduces relations between the coefficients with different values of m. In this case it is convenient to introduce new

harmonics, called Kubic harmonics, defined as

$$K_{l,1}=\sum_m a_{l,1,m}\,C^g_{l,m}\,. \tag{6}$$

The coefficients $a_{l,1,m}$ have been determined to $l=60$.[23,28] By differentiating Eqs. (3a) and (3b) with respect to E we find

$$\left(\frac{\partial A(\theta,\varphi)}{\partial E}\right)_{\theta,\varphi}=\sum_{l,m}\left[\gamma'^{g}_{l,m}\,C^g_{l,m}(\theta,\varphi)+\gamma'^{u}_{l,m}\,C^u_{l,m}(\theta,\varphi)\right], \tag{7a}$$

$$2k\left(\frac{\partial k}{\partial E}\right)_{\theta,\varphi}=\sum_{l,m}\left[\beta'^{g}_{l,m}\,C^g_{l,m}(\theta,\varphi)+\gamma'^{u}_{l,m}\,C^u_{l,m}(\theta,\varphi)\right], \tag{7b}$$

where

$$\gamma'_{l,m}=\frac{\partial\gamma_{l,m}}{\partial E}\quad\text{and}\quad\beta'_{l,m}=\frac{\partial\beta_{l,m}}{\partial E}\,.$$

It is easy to show that the coefficients $\beta_{l,m}$ and $\beta'_{l,m}$ completely determine the three components of the Fermi velocity.[25] We will require Eqs. (7a) and (7b) when deducing the band mass m^*_B, from the band-structure radii and velocities.

In cases where the Fermi surface is nearly ellipsoidal the convergence of Eqs. (3) and (7) may be greatly improved by rescaling the principal axis of the ellipsoid so that it is mapped into a sphere. The $X4$ pocket is an example in point. We define the new coordinate system by $k'_x=k_x$, $k'_y=k_y$, $k'_z=\gamma k_z$, and define the transformation T which changes the polar angle θ into $\theta'=T\theta$ according to

$$T\theta=\tan^{-1}\left(\tan\theta/\gamma\right), \tag{8a}$$

$$T^{-1}\theta=\tan^{-1}\left(\gamma\tan\theta\right). \tag{8b}$$

It has been shown that the behavior of the area and radii under this mapping are given by[26]

$$A'\left(T^{-1}\theta,\varphi\right)=\left[\gamma^2+(1-\gamma^2)\cos^2\theta\right]^{1/2}A(\theta,\varphi)\,, \tag{9a}$$

$$k'^2(T\theta,\varphi)=\left[1+(\gamma^2-1)\cos^2\theta\right]k^2(\theta,\varphi)\,. \tag{9b}$$

Similar formulas exist for the effective mass and Fermi velocity case.[27]

In cases where the Fermi surface is open one requires a representation which is invariant under the operations of the space group, i.e., translations as well as rotations. A representation of the required symmetry is a three-dimensional Fourier series of the form

$$F(\vec{k})=\sum_{\vec{R}} C_{\vec{R}}\,e^{i\vec{k}\cdot\vec{R}}\,, \tag{10}$$

where the $\vec{R}$ are the vectors of the real-space lattice, i.e., $\vec{R}=l\,\vec{a}+m\,\vec{b}+n\,\vec{c}$, where $\vec{a}$, $\vec{b}$, and $\vec{c}$ are the primitive translation vectors. The equation $F(\vec{k})=0$ defines a surface and the solution of this implicit equation yields this surface. If one has some initial set of $C_{\vec{R}}$ which approximate the Fermi surface (which may be obtained from a band structure) then a rapidly convergent iterative procedure may be applied which will generate a new set of $C_{\vec{R}}$ which better fit the experimental data.[30] By regarding the $C_R(a,\,E)$ as dependent on the energy E, or lattice constant a, one may determine how the surface changes with these parameters by fitting effective mass or pressure-dependent dHvA areas, respectively.[31–34]

In performing the area-to-radii inversions for the Γ-centered surface the Kubic-harmonic expansions were carried out to order $l=30$. An error in the orientation of the specimen by an angle $\Delta\theta$ results in an error in the expansion coefficient $\gamma_{l,m}$ or order $\Delta\gamma_{l,m}/\gamma_{l,m}\sim\cos\left[l(\theta+\Delta\theta)\right]$ which for $l=30$ amounts to an error of order 1 for $\Delta\theta=2^\circ$ (which is the usual experimental accuracy). Thus, a technique to improve the accuracy of the orientation by about a factor of 10 is clearly necessary. A technique which allows one to orient the dHvA data, for the rotation of the magnetic field in an arbitrary plane, has been developed which makes use of the known crystal symmetry (cubic in this case) of the data.[35] Data in arbitrary planes are necessary in carrying out high-order expansions.[13,23,27]

IV. EXPERIMENTAL TECHNIQUE AND PROCEDURES

The measurements to be reported here were carried out using the large-amplitude low-frequency field-modulation technique,[36,37] and most of the techniques for enhancing specific dHvA frequencies were employed. The experimental apparatus has been discussed elsewhere.[13,37] Briefly, it consists of a 72-kG superconducting solenoid together with either ^{3}He or ^{4}He evaporative cooling. To obtain effective masses using the temperature dependence of the dHvA amplitude, precise measurements of the vapor pressure are required. Such measurements were performed using a Texas Instruments precision pressure gauge.

The samples were right circular cylinders 1 mm in diam by 4–7 mm in length and were grown from Johnson Matthey[38] 99.999 pure Pd using a rf-heated floating zone refiner of special design.[39,40] This was followed by an air-annealing procedure which resulted in residual-resistance ratios of greater than 4000 in many cases.[40] The palladium-cobalt alloys were prepared by melting the constituents into a rod using a water-cooled silver boat.[40,41] The rod was then zone stretched[40] into a 1-mm-diam single crystal. All samples were cut to length using a moving-wire spark cutter.

In the data to be reported here, the magnetic field was not constrained to lie in planes of mirror symmetry since the expansion in Kubic harmonics to values of $l>16$ requires additional data.[23] We will now discuss the parameters which were used in the present experiment to specify the orientation

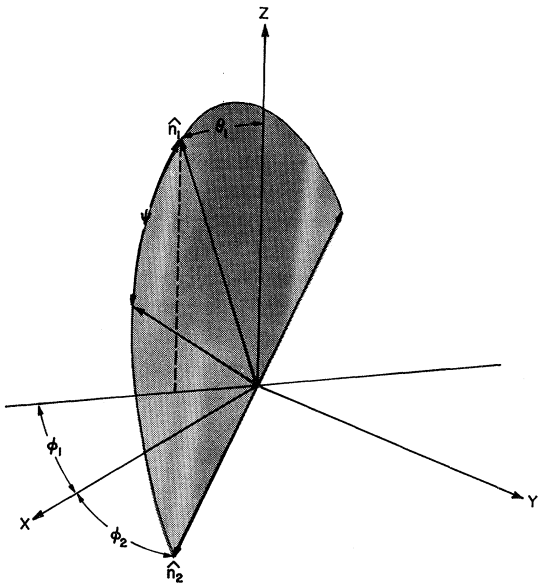

FIG. 6. Plane of rotation of the sample as specified by the vectors $\hat{n}_1$ and $\hat{n}_2$ (see text).

of the sample for the rotation of the magnetic field in an arbitrary plane (which however includes the sample axis). These parameters are illustrated in Fig. 6. A sample rotator positions the sample relative to the solenoid axis or, equivalently, relative to the magnetic field direction. The sample axis is specified by the unit vector $\hat{n}_1$ having polar angles θ_1 and φ_1 relative to the crystal axes measured in a right-handed coordinate system as shown in Fig. 6. θ_1 is the polar angle from the sample axis to the nearest [001] crystal axis (called the z axis). φ_1 is the azimuthal angle of the sample measured from one of the other two remaining [100] axes (called the x axis). This completes the specification of the sample axis. To define a plane of rotation of a sample we must specify another vector $\hat{n}_2$ not colinear with $\hat{n}_1$. The choice of the second vector is somewhat arbitrary since any two (noncolinear) vectors are sufficient to define the plane of rotation. We chose the second vector $\hat{n}_2$ as the intersection of the plane of rotation of the magnetic field with the x-y plane of the crystal (the y axis being the third [010] axis). θ_2 and φ_2 are the polar coordinates of this vector, where θ_2 is obviously 90°. The angle φ_2 is however nonunique since the crystal x-y plane and the plane of rotation of the sample intersect at two values of φ_2, one being 180° greater than the other. The specification is made unique in the following way. We denote the experimental angle of the sample rotator as ψ. The second vector (x-y plane intersection vector) is chosen in the direction of *increasing* values of ψ as the sample axis is turned away from the magnet axis. This then defines φ_2. The determination of the zero of the experimental angle ψ is accomplished by observing the disappearance of the inductive pickup when the pickup coil (sample axis) is perpendicular to the vertical modulation coil axis (magnet axis). The calibration constant of the angle ψ (number of experimental dial divisions per degree) is found by observing the number of dial divisions between the two null points at $\psi = \pm 90°$. The following effect requires the introduction of another parameter. Owing to a small amount of clearance in the bearings of the sample rotator, some tipping of the rotor occurs which in practice amounts to $\sim \pm \frac{1}{2}°$. The result is that the magnetic field moves on a cone of half-angle α rather than on a great circle (where $\alpha \sim 90°$) of the unit sphere relative to the crystal axis. The angle α is defined so that it is less than 90° in the hemisphere intersecting the vector $\hat{n}_1 \times \hat{n}_2$. In doing accurate work it is necessary to include an additive correction for the data in one plane relative to another since the relative accuracy of data taken with field rotations exceeds the absolute accuracy by about an order of magnitude. This additive constant A_0 was also determined from the data. We thus have five parameters to determine: A_0, θ_1, φ_1, φ_2, and α. θ_1, φ_1, and φ_2 can be approximately determined ($\pm 2°$) from x rays. We have developed a variation procedure for improving the accuracy of θ_1, φ_1, φ_2 and for determining α, all to order 0.2°, by using the cubic symmetry of the data.

V. EXPERIMENTAL RESULTS

A. General

The dHvA frequencies were studied for the magnetic field in seven nonsymmetry crystallographic planes, and these will be designated by the letters a–g. In addition, the dHvA effective masses were studied in planes c–g. Plane d is quite close to a (110) plane. dHvA data associated with all three sheets of the surface were observed. The most detailed data are for the Γ-centered and X-centered sufaces as the amplitude was usually much larger for these sheets. The orientation of the data was initially carried out using x-ray techniques with an accuracy of approximately 2°. The final orientations were however carried out using the cubic symmetry of the data on the Γ-centered surface[35] as these data were the most accurate and complete. Initially, a single plane was oriented by varying the parameters in the order θ_1, α, φ_2, φ_1. More planes were then added one at a time by first varying the orientation parameters of the new plane followed by successive variation of the parameters of all current planes. This was continued until all seven planes were self-consistently oriented. Parameters A_0 were included for all but the first plane. Table I contains the orientation parameters

TABLE I. Specification angles for the planes in which dHvA data were taken.

Run	θ_1	φ_1	θ_2	φ_2	α	ψ_0[a]
a	30.6205	24.8986	90.0	214.8962	89.8056	92.4
b	30.4366	26.7634	90.0	201.2240	89.7267	92.4
c	22.0860	56.7864	90.0	−69.2451	90.1942	92.4
d	72.9099	45.5000	90.0	225.7000	89.7000	92.4
e	45.9450	28.3266	90.0	46.6716	90.6575	92.4
f	41.0879	71.2377	90.0	70.1402	89.2720	92.4
g	42.1259	−19.0091	90.0	66.0522	89.9176	92.4

[a]Value of ψ for the field along the crystal axis (i.e., along $\hat{n}_1$ in Fig. 6) for $\alpha = 90.00$. The calibration of the angle monitor does not correspond exactly to rotation in degrees; a change of 10 units in ψ corresponds to a rotation of the sample holder of 10.37 deg.

obtained for the seven planes. These parameters are on the whole accurate to about 0.2°. The values of A_0 are not reported as the data to be presented here include that correction. The traces in Fig. 7 show the path traversed by the magnetic field on the stereogram for the seven data cones studied. The divisions along the traces correspond to the divisions on the data to be presented shortly. If these traces are folded into the basic $\frac{1}{48}$th of the unit sphere the coverage is so complete that any direction on the unit sphere lies within 3° of a direction where the dHvA area was determined. The areas and radii to be presented here are all measured in units of a_0^{-2} and a_0^{-1}, respectively, where a_0 is the Bohr radius ($a_0 = \hbar^2/me^2 = 0.5292$ Å). The effective masses are measured in units of the free-electron mass. The dHvA frequency data were usually taken at ^{3}He temperatures ($T \cong 0.35$ K) in order to maximize the signal-to-noise ratio. Effective-mass data on the other hand were usually taken at ^{4}He temperatures (1.0–2.2 K) since better thermometry was achievable due to the excellent temperature equilibrium obtained with superfluid ^{4}He. If signal-to-noise ratio did not permit ^{4}He thermometry, then temperature measurement could be made at ^{3}He temperatures with, however, some loss in accuracy. Wherever possible, field rotations were performed such that data might have high relative accuracy. The sample rotator was such that 80 or more oscillations per deg were resolvable. The data reported for the Γ-centered surface were largely obtained from field rotations. For heavy-mass directions, as encountered on the open surface, the noise introduced by the act of rotating the sample required that the dHvA frequencies be obtained from a field sweep. In any case, at least one field sweep is required to normalize the field-rotation data although in practice these were usually performed at least every 10°.

B. Γ-Centered Electron Surface

The dHvA areas for the Γ-centered surface observed in runs *a–f* are shown in Figs. 8(a)–8(f). Planes *e* and *g* are essentially equivalent except that the axis of the crystal for run *g* was more favorable for the observation of orbits on the open-hole surface near [110]. Complete area data for the Γ-centered electron surface were obtained in both runs in order to determine the exact orientations of the planes. For the magnetic field in the vicinity of [111] the surface supports two extremal cross sections, the smaller of these being associated with the central section. We have taken the central-section data from these seven planes and fitted it to Kubic harmonics[23] according to Eq. (3a). Fits were carried out for $l = 26$, 28, and 30 corresponding to 21, 24, and 27 expansion coefficients γ_{il}, respectively. The predicted radii varied no more than a few parts per thousand for these three fits. The $l = 26$ term fit to the data is shown as the solid lines in Figs. 8(a)–8(g). We have generated the contours of constant area in the basic $\frac{1}{48}$th of the unit sphere and these are shown in Fig. 9. Using Eq. (5) we may generate the coefficients β_{il} of Eq. (3b). The expansion coefficients γ_{il} and β_{il} are listed in Table II. Figure 10 shows the Fermi radius of the Γ-centered surface in the (100) and (110) planes. Shown for comparison are the RAPW calculations of Andersen and Mackintosh[10] together with the APW-Relativistic Interpolation Scheme calculations of Mueller *et al.*[12] On the whole the agreement is satisfactory although an effort to improve the agreement appears worthwhile. Such an effort might proceed along several different lines. One might try to improve the potential (including the exchange term) in the first principal calculations. Alternatively one might try to generate a set of phase shifts $\delta_l(E_F)$ which would best represent the surface. This latter would clearly show whether "outside the muffin-tin corrections" are necessary. Figure 11 shows the contours of constant radius.

Figure 12(c)–12(f) shows the cyclotron effective masses m^* measured in runs *c–f* for the Γ-centered electron surface. As in the corresponding case for the extremal area, there are two cyclotron masses for the field near [111]. Observe that the cyclotron mass is rather isotropic except for the field near [110] [near 65 in Fig. 12(c), 75 in Fig. 12(d), and 140 in Fig. 12(e)], where the mass becomes quite anisotropic. Attempts to fit the mass data to Kubic harmonics according to Eq. (7a) for $l \leq 30$ were unsuccessful in the sense that the predicted values of $k(\theta, \varphi)[\partial k(\theta, \varphi)/\partial E]$ obtained using Eq. (7b) varied considerably. (A higher-order fit does not appear justified as the scatter in the experimental data tends to be overemphasized.) The above experience suggests that something peculiar is occurring in the angular dependence of $k(\theta, \varphi) \times [\partial k(\theta, \varphi)/\partial E]$. To check this point we examined

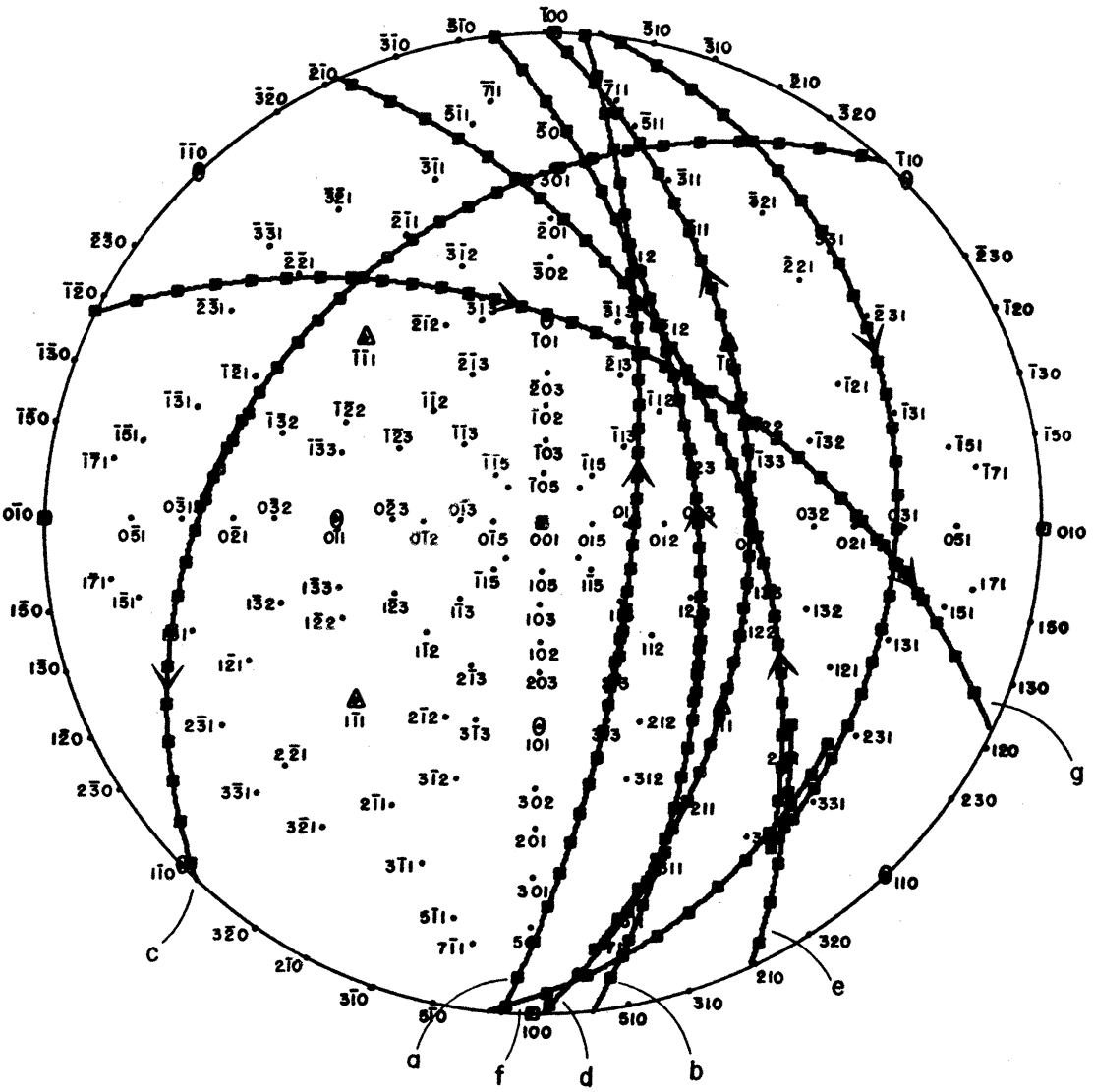

FIG. 7. Stereographic plot of the seven planes (cones) a–g in which the dHvA effect was studied in Pd. The units along the traces of the magnetic field are such that a change of 5 in the experimental coordinate ψ corresponds to a change in angle of 5.185 deg.

the angular dependence of $k(\theta, \varphi)[\partial k(\theta, \varphi)/\partial E]$ as determined in the band-structure calculations. The values of $\partial k(\theta, \varphi)/\partial E\,(=v_k^{-1}$, where v_k is the radial component of the Fermi velocity) were calculated from values of $k(\theta, \varphi, E)$ on two energy shells in the vicinity of the Fermi level. Figure 13 shows the values of $k(\theta, \varphi)[\partial k(\theta, \varphi)/\partial E]$ in the (100) and (110) planes as calculated by Andersen and Mackintosh[10] and by Mueller *et al.*[12] The source of our problem is now obvious. Note that $k(\theta, \varphi)[\partial k(\theta, \varphi)/\partial E]$ is reasonably smoothly varying except for a small range of angles near [100] and [111] where it decreases dramatically. By examining the relative fraction of the conduction-electron wave function which is d like or s like (plane-wave-like) it develops that the wave function is mostly d like over the majority of the Γ-centered surface except near [100] and [111] where it is mostly s like.[12] Since the velocity is considerably larger for s-like electrons, this results in the dramatic decrease in $k(\theta, \varphi)[\partial k(\theta, \varphi)/\partial E]$ near [100] and [111]. It is clear that a rather high-order fit would be required to reproduce the angular dependence shown in Fig. 13. Since the experimental data are not accurate or complete enough to justify such a high-order fit this suggests that we reverse the procedure and use the band-structure values of $k(\theta, \varphi)[\partial k(\theta, \varphi)/\partial E]$ to predict the unenhanced cyclotron effective mass

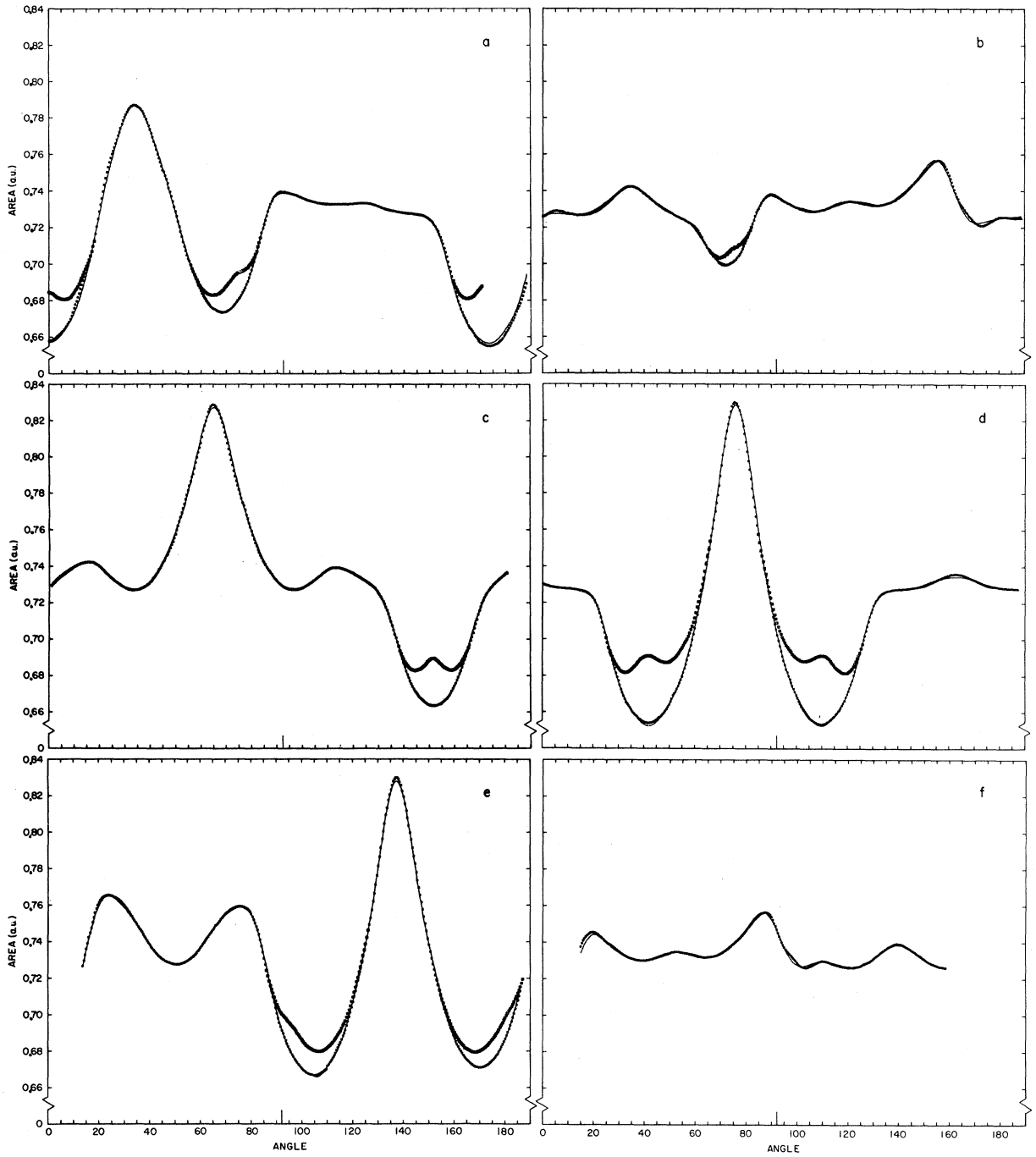

FIG. 8. Angular dependence of the extremal area for the Γ-centered electron sheet of the Fermi surface of Pd observed in planes *a–f*. Solid line shows the $l=26$ (21-term) Kubic-harmonic fit. The angular scale corresponds to the experimental coordinate ψ as shown in Fig. 7.

$m^*(\theta, \varphi)$. We have performed an $l=60$ expansion [corresponding to 91 terms in Eqs. (7a) and (7b)] by fitting values of $k(\theta, \varphi)[\partial k(\theta, \varphi)/\partial E]^{12}$ in the $\frac{1}{16}$th of the unit sphere and on a grid of $2\frac{1}{2}^\circ$ in θ and $7\frac{1}{2}^\circ$ in φ. This fit is shown as the solid line in Fig. 13. Using Eq. (5) we can calculate $m^*(\theta, \varphi)$ from Eq. (7a) and the dashed line in Figs. 12(c)–12(f) shows the result. Note that we do not expect these to agree with experiment as we have not accounted for any of the mass-enhancing effect although we do expect the anisotropy to be similar. Taking these factors into account the experimental and theoretical

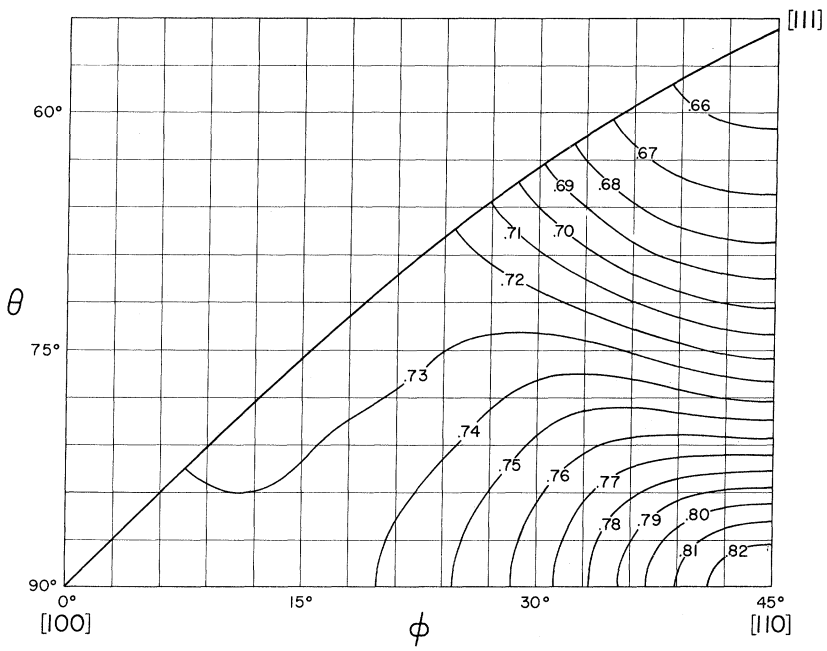

FIG. 9. Contours of constant area for the Γ-centered electron sheet of the Fermi surface of Pd in the basic triangle.

masses appear to be in satisfactory agreement. Although an $l = 26$ (21 term) fit does not, in our estimation, yield an accurate inversion, it does reproduce the gross features of the data. For this reason we have used the $l = 26$ fit to generate approximate contours of constant mass which are shown in Fig. 14(a).

For all experimental planes studied, the amplitude of the dHvA oscillations associated with the Γ-centered surface was observed to vanish at certain magnetic field directions.[42] This is due to the effects of spin splitting as discussed in Sec. III. In particular this occurs when $[m^*(\theta, \varphi)/m_s(\theta, \varphi)] = r + \frac{1}{2}$, where we have defined a spin mass $m_s(\theta, \varphi) \equiv [2m_0/g(\theta, \varphi)]$. We have remapped the magnetic

TABLE II. Area and cyclotron-effective-mass expansion coefficients for the Γ-centered electron sheet of the Fermi surface of Pd.

i	l	β_{il}	γ_{il}	β'_{il}	γ'_{il}
1	0	2.591 00	0.824 74	7.528 52	2.396 40
2	4	0.038 25	0.032 47	−0.151 51	−0.128 60
3	6	−0.113 92	0.116 04	−0.318 21	0.324 12
4	8	0.015 34	0.017 86	0.022 98	0.026 75
5	10	0.003 29	−0.004 25	0.099 30	−0.128 44
6	12	0.010 22	0.014 42	0.059 33	0.083 72
7	12	−0.021 00	−0.029 63	−0.028 28	−0.039 91
8	14	−0.006 32	0.009 60	−0.021 22	0.032 25
9	16	−0.000 28	−0.000 45	−0.037 24	−0.060 36
10	16	0.003 41	0.005 53	0.051 26	0.083 09
11	18	−0.002 47	0.004 24	0.024 46	−0.041 98
12	18	0.006 58	−0.011 29	0.002 16	−0.003 70
13	20	0.002 35	0.004 24	−0.010 98	−0.019 83
14	20	−0.003 07	−0.005 54	0.003 41	0.006 15
15	22	0.000 22	−0.000 41	0.025 23	−0.047 75
16	22	−0.001 55	0.002 93	−0.000 79	0.001 50
17	24	0.000 47	0.000 93	−0.000 53	−0.001 05
18	24	−0.000 72	−0.001 43	0.020 05	0.039 59
19	24	0.002 55	0.005 03	−0.039 47	−0.077 95
20	26	−0.001 75	0.003 60	0.005 44	−0.011 16
21	26	0.001 70	−0.003 49	−0.010 10	0.020 75

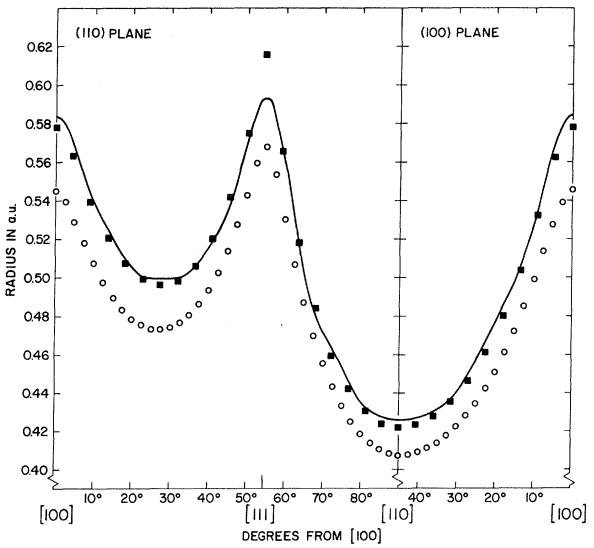

FIG. 10. Solid line shows the radius of the Γ-centered electron sheet of the Fermi surface of Pd in the principle crystal planes. The squares are the calculation of Andersen and Mackintosh (Ref. 10), while the circles are the APW-Interpolation Scheme calculation of Mueller *et al.* (Ref. 12).

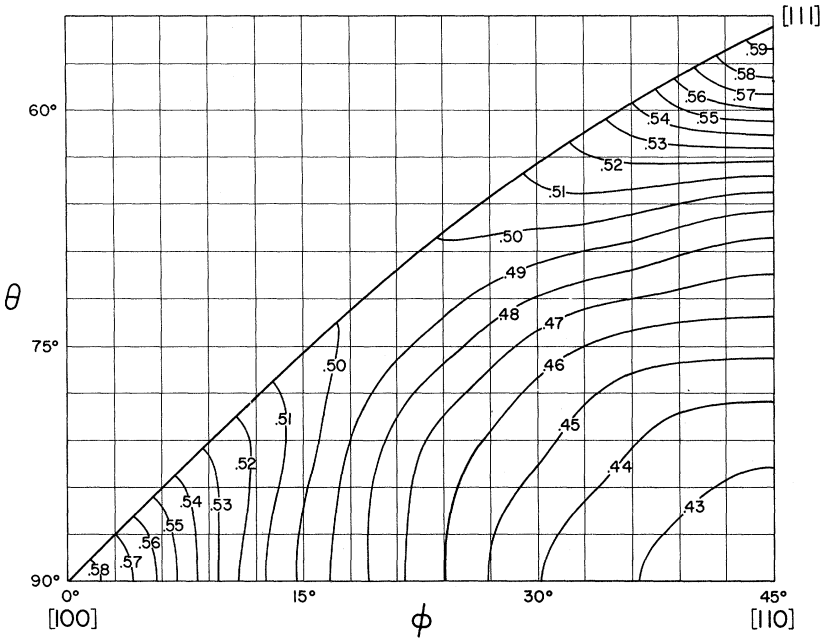

FIG. 11. Contours of constant radius for the Γ-centered electron sheet of the Fermi surface of Pd in the basic triangle.

field direction, where these "spin-splitting zeros" occur into the basic $\frac{1}{48}$th of the unit sphere and these data are shown in Fig. 14(b). The heavy solid line and the short dashed-line segment connecting these points trace out the contours in the basic $\frac{1}{48}$th of the unit sphere where the dHvA amplitude should vanish due to spin splitting. Such a contour cannot end abruptly in the center of the basic triangle as the dashed segment appears to do. This point has, however, been discussed in detail elsewhere.[13,43] If the g factor (spin mass) were isotropic, then the heavy solid line of Fig. 14(b) would have to run

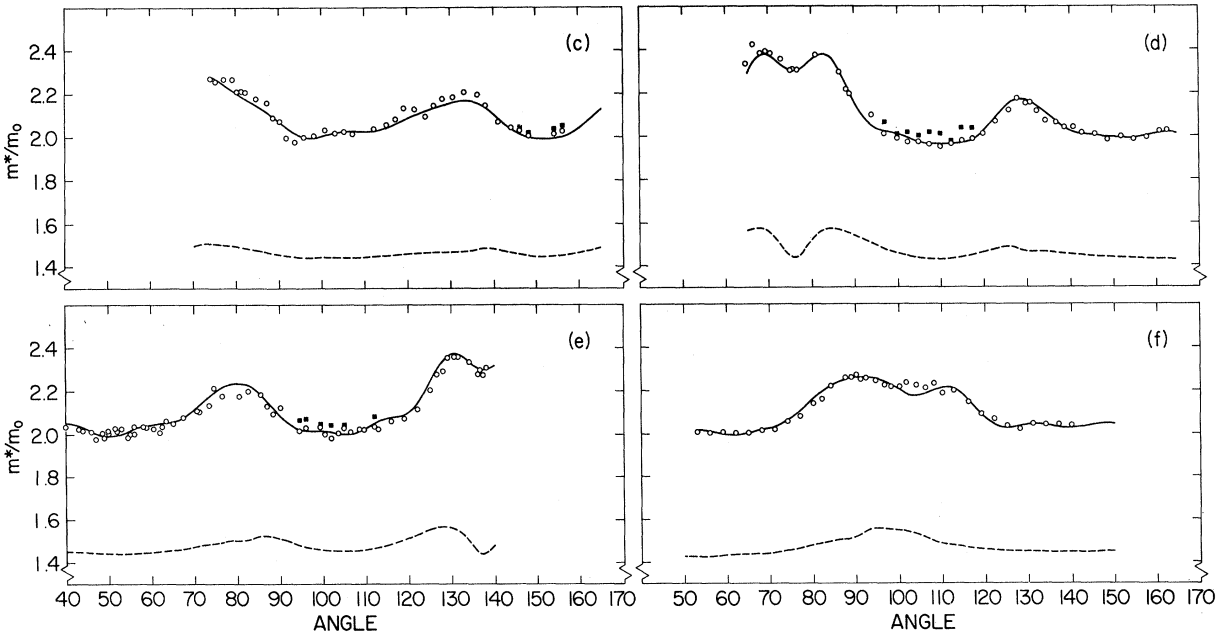

FIG. 12. Angular dependence of the cyclotron effective masses for the Γ-centered electron sheet of the Fermi surface of Pd observed in planes c–f. Solid line shows the $l=26$ (21-term) Kubic-harmonic fit. Dashed line shows the unenhanced cyclotron effective masses predicted from the band-structure calculation of Mueller *et al.* (Ref. 12) according to the procedure described in the text.

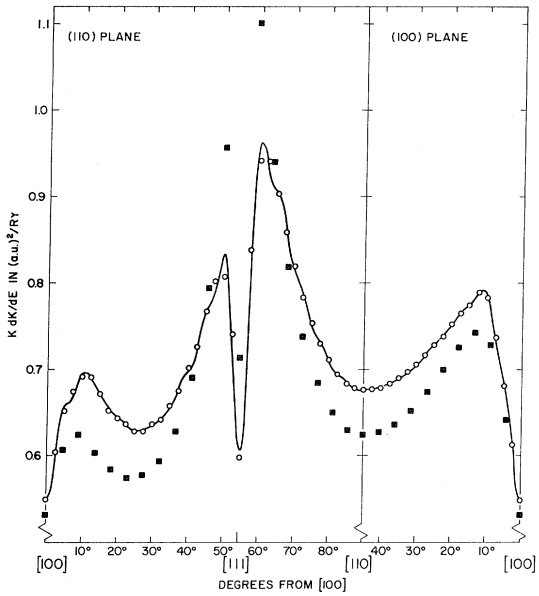

FIG. 13. Angular dependence, in the principle crystal planes, of $k(\theta, \varphi)\,[\partial k(\theta, \varphi)/\partial E]$ for the Γ-centered electron sheet of the Fermi surface of Pd. The circles are the calculation of Mueller *et al.* (Ref. 12) and the squares are the calculations of Andersen and Mackintosh (Ref. 10). The solid line shows an $l=60$ (91-term) Kubic-harmonic fit to the calculations of Mueller *et al.* as described in the text.

parallel to one of the effective-mass contours. Thus we conclude that the g factor in Pd differs from 2 and is somewhat anisotropic. A similar situation exists in Pt.[43,44] If we choose a value for r which would place the g factor closest to its free-space value of 2.0 then we can derive values of the g factor along the contours of Fig. 14(b) by using the interpolated cyclotron mass value [which are shown as the light lines in Fig. 14(b) for reference]. Such a calculation shows that the g factor ranges from 2.13 to 2.44. The fact that the g factor differs from 2 should be accounted for when making estimates of the density of states (from the Pauli susceptibility) and in turn the Stoner enhancement factor. Recent theory indicates, however, that the dHvA g factor likely contains the Stoner factor.[45]

Using the 21-term fits to the radii and velocities, we can compute the number of carriers and density of states for the Γ-centered electron sheet by direct numerical integration.[13,28] We obtain $n(E_F) = 3.79\times10^{-3}\,a_0^{-3}$ or 0.376 e/atom for the number of carriers and $N(E_F) = 5.31\times10^{-2}\,a_0^{-3}$ Ry^{-1} or 5.28 e/atom Ry for the density of states.

We have collected the areas, radii, and cyclotron effective masses for the [100], [111], and [110] directions in Table III. Shown for comparison are the corresponding quantities as calculated by Andersen and Mackintosh[10] using the RAPW technique.

C. X-Centered Pocket

dHvA oscillations arising from the X-centered hole pocket were observed in all seven experimental planes. Figure 15 shows the observed dHvA areas for the magnetic field in plane d. Since this plane is almost a (110) plane the two nonprinciple area branches are nearly degenerate while the principle branch approximates quite closely to the corresponding values in this mirror plane. Detailed analysis of all the data using the spherical-mapping fitting procedure shows that the pockets are roughly ellipsoidal in shape with small but significant deviations. The solid line in Fig. 15 shows the results of a fit using six terms through $l=6$. The parameters for this fit are given in Table IV.

Cyclotron effective masses on the ellipsoidal pocket were measured for selected field directions in planes c–g. Table V lists the observed masses and the corresponding masses calculated from a six term $l=6$ spherical-mapped fit to the data. Although the mass data do not have quite the accuracy of the area data, significant departures from ellipsoidal behavior outside of experimental error were still detectable thus necessitating the six-term fit. The parameters for this fit to the mass data are also given in Table IV.

Using the parameters in Table IV, the number of carriers and density of states per ellipsoid were calculated by direct numerical integration.[13,28] For the number of carriers per ellipsoid we find $n(E_F) = 1.81\times10^{-5}\,a_0^{-3}$ or 1.80×10^{-3} holes/atom. For the density of states per ellipsoid we find $N(E_F) = 3.88\times10^{-3}\,a_0^{-3}$ Ry^{-1} or 3.85×10^{-1} holes/atom Ry. Table III compares the experimental data at [100], [111], and [110] with the corresponding quantities as calculated by Andersen and Mackintosh.[10]

D. Open-Hole Surface

Although the complicated shape of the open-hole surface (see Fig. 3 and Sec. II above) is expected to support many dHvA orbits, only oscillations associated with the α and γ orbits were observed in the present experiment. Figure 16 shows the α-orbit dHvA areas for the magnetic field in plane b. dHvA oscillations arising from the α orbit were observed in all seven experimental planes and cyclotron effective mass data were obtained for a limited set of magnetic field directions in planes e, f, and g. Table VI lists the observed cyclotron mass data. Fits to both the area and mass data resulted in the contour maps of the area in Fig. 17 and the mass in Fig. 18. (A detailed discussion of the fitting procedure for orbits on the open-hole surface is given in Ref. 13). Table VII gives the expansion coefficients. Shown also in Fig. 18 are the directions where the amplitude of the dHvA oscillation vanished due to spin splitting. Since

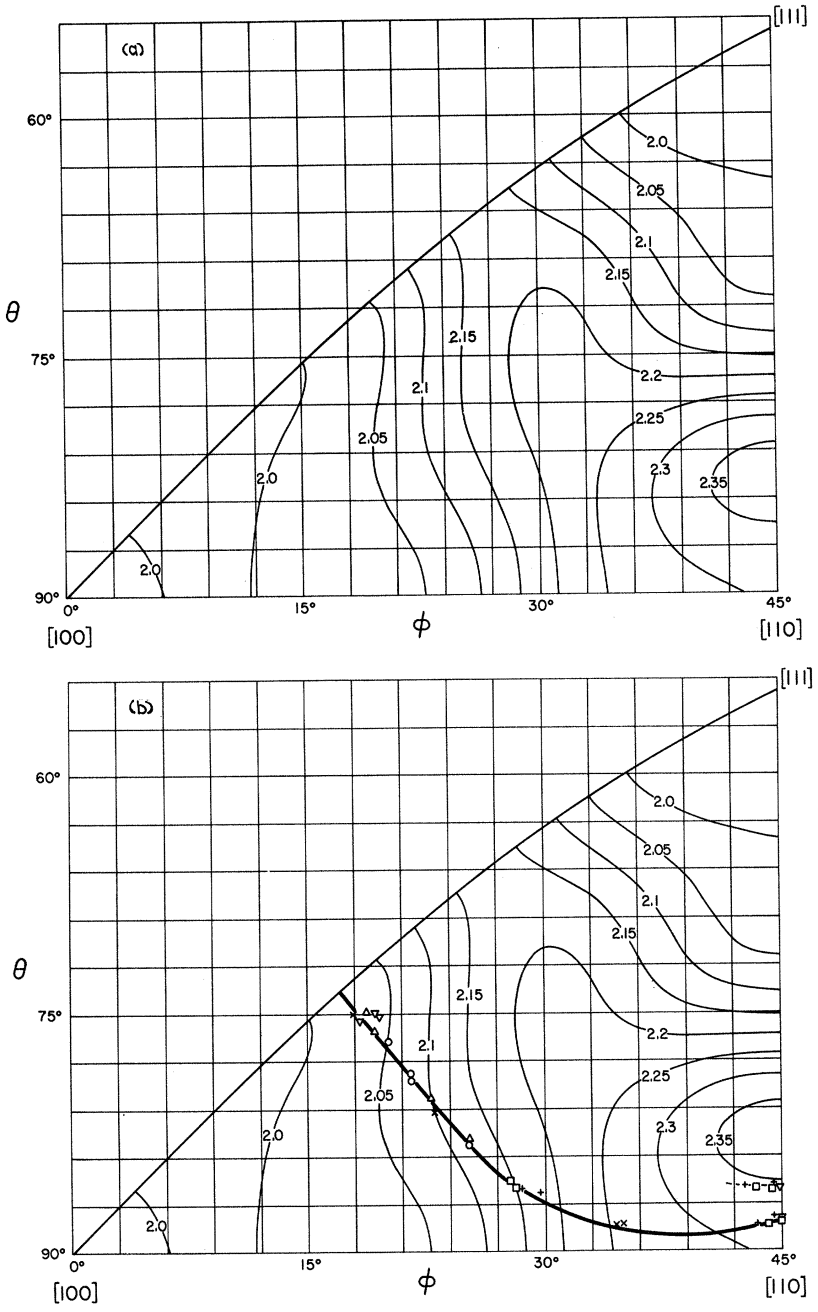

FIG. 14. (a) Contours of constant cyclotron effective mass for the Γ-centered electron sheet of the Fermi surface of Pd in the basic triangle. (b) Contour on which spin-splitting zeros were observed for the Γ-centered electron sheet of the Fermi surface of Pd in the basic triangle. The short dashed-line segment shows an incomplete spin splitting contour (see text). The light solid lines show the cyclotron effective mass contours for reference.

the spin-splitting contour lies on a cyclotron effective mass contour, the contours of constant g likely run parallel to the contours of constant cyclotron effective mass.

dHvA oscillations arising from the γ orbit were observed only over a limited range of magnetic-field directions in plane g. Figure 19 shows this data. Cyclotron effective masses were determined at 108 and 111 giving values of 6.0 ± 0.3 and 6.2 ± 0.3, respectively.

Our values for the density of states of the Γ-centered electron sheet and X-centered hole pocket can be combined with the measured heat-capacity density of states to determine the density of states of the open-hole sheet. Using the value $N(E_F) = 54$ states/atom Ry for the total electronic density of states[8] we find $N(E_F) = 47.6$ holes/atom Ry for the open-hole sheet. By invoking charge neutrality we can calculate the number of carriers in the open-hole sheet for which we find $n(E_F) = 0.371$ holes/atom.

Table III compares the experimental data at

TABLE III. Comparison of experimental results with RAPW band calculation of Andersen and Mackintosh. [a]

	Extremal area (a.u.)		Cyclotron mass m^*/m_0			Fermi momentum (a.u.)		Fermi velocity (radial component) (a.u.)
	Expt	Theor	Expt	Theor	Ratio	Expt	Theor	Expt
Γ-Centered electrons								
[100]	0.735	0.723	2.02	1.34	1.51	0.584	0.579	
[110]	0.828	0.826	2.30	1.47	1.56	0.426	0.422	
[111]	0.652	0.645	1.96	1.35	1.45	0.593	0.616	
X-Centered hole pocket								
[100]	0.0153	0.0170	0.631	0.41	1.54	0.106	•••	0.085
	0.0238	0.0264	1.360[b]	0.70	1.94	0.069	•••	0.182
[110]	0.0240	0.0265	1.030	0.65	1.58	0.071	•••	0.282
	0.0185	0.0206	0.777	0.53	1.47	0.084	•••	0.136
[111]	0.0201	0.0225	0.868	0.55	1.58	0.079	•••	0.268
Open-hole surface								
[100] α orbit	0.072	0.0685	2.40	1.37	1.75			
[110] β orbit	•••	0.320	•••	9.1	•••			
[110] γ orbit	0.201	•••	6.0	•••	•••			

[a]Reference 10.
[b]Extrapolated with six-term fit.

[100] and [110] with the corresponding quantities as calculated by Andersen and Mackintosh.[10]

VI. EXCHANGE SPLITTING

It is well known that the addition of as little as a few tenths of an atomic percent of cobalt or iron is sufficient to cause palladium to become ferromagnetic at low temperatures.[1,2] It is important to ascertain whether this ferromagnetism arises from a large effective local moment on the impurity ions or from an exchange splitting of the electronic bands, resulting in unequal population of the spin-up and spin-down bands. The dHvA effect provides a sensitive test to distinguish between these two cases. In the localized case, the highly polarized impurity ion would scatter the conduction electrons strongly, resulting in a very large reduction in the dHvA amplitude and a rapid disappearance of the effect with increasing impurity concentration. The exchange split case, however, would differ from this behavior in several respects. First, the electronic scattering would be less, resulting in the observation of the dHvA effect in alloys with relatively greater cobalt or iron concentration. In addition, the Fermi surfaces of the exchange split bands would now have slightly different extremal

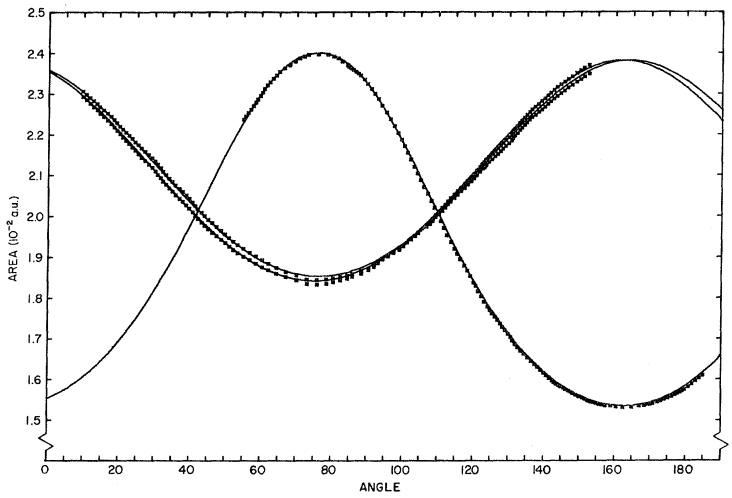

FIG. 15. Angular dependence of the extremal area for the *X*-centered ellipsoidal pocket of the Fermi surface of Pd observed in plane *d*. Solid lines show the $l=6$ (six-term) fit. The angular scale corresponds to the experimental coordinate ψ as shown in Fig. 7.

TABLE IV. Area and cyclotron effective mass expansion coefficients for the X-centered hole pocket of the Fermi surface of Pd.

		Area $\gamma = 0.641$		Mass $\gamma = 0.612$	
i	l	$10 \cdot \beta_{il}$	$10 \cdot \gamma_{il}$	β'_{il}	γ'_{il}
1	0	0.548 60	0.174 62	2.423 43	0.771 40
2	2	0.001 59	−0.001 01	−0.105 61	0.067 24
3	4	−0.002 93	−0.002 49	0.032 51	0.027 60
4	4	−0.001 55	−0.001 31	0.123 36	0.104 71
5	6	0.000 12	−0.000 12	−0.013 11	0.013 35
6	6	−0.000 72	0.000 74	−0.047 66	0.048 55

areas associated with corresponding spin-up and spin-down sheets. This effect would be observable as a beating in the dHvA oscillations, with the beat frequency providing a measure of the magnitude of the exchange splitting. Another consequence of the exchange splitting would be the disappearance of the spin-splitting zeros which are observed in the pure material. Spin-splitting zeros cannot occur since the oscillations arising from the spin-up and spin-down sheets of a given surface no longer have identical frequencies as they do in the pure materials.

TABLE V. Cyclotron effective masses on the X-centered hole pocket of the Fermi surface of Pd.

Plane	ψ	θ	φ	Expt m^*	Calc[a] m^*
c	105	17.98	19.82	0.658	0.655
d	41.1	54.60	46.30	0.870	0.869
	75	90.96	45.41	1.000	1.030
	83	45.16	−10.38	0.766	0.777
	92	73.33	45.19	1.029	1.004
	98	49.27	−30.89	0.810	0.819
	110	54.66	44.87	0.862	0.868
	131	32.89	44.14	0.727	0.711
	144	19.42	42.95	0.655	0.659
	162.5	0.97	−31.55	0.624	0.631
e	15	41.12	−110.31	0.752	0.756
	24	33.21	−102.07	0.722	0.712
	60	20.85	−15.97	0.651	0.662
	95	48.66	29.08	0.814	0.813
	125	77.68	41.89	1.036	1.021
	131	44.25	99.21	0.774	0.771
	136.2	88.71	45.56	1.049	1.030
	136.5	89.01	45.66	1.039	1.030
f	42	11.31	−118.39	0.636	0.640
	53	1.70	152.67	0.642	0.631
	75	23.10	74.24	0.668	0.670
	98.5	47.43	72.01	0.808	0.797
	120	27.34	−49.01	0.688	0.687
	147	20.69	22.32	0.663	0.662
g	105	90.15	−45.54	1.033	1.030
	109	86.19	−44.29	1.015	1.029
	150	70.26	47.31	0.966	0.989
	155	73.95	51.14	1.010	1.011

[a]Using the expansion coefficients of Table IV.

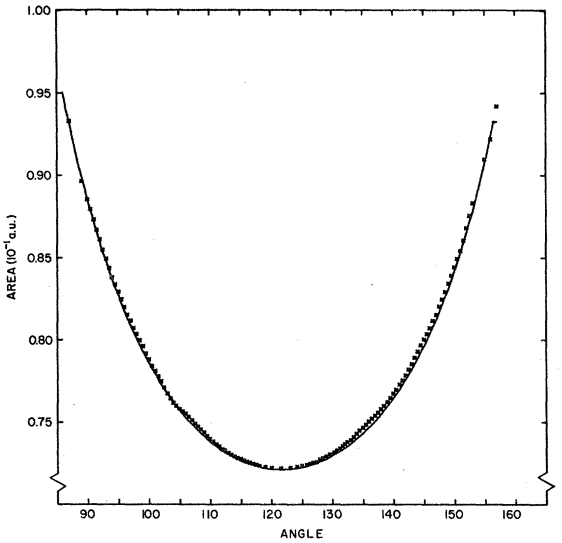

FIG. 16. Angular dependence of the extremal area for the α orbit on the open-hole sheet of the Fermi surface of Pd observed in plane b. Solid line shows the $l=6$ (six-term) fit to the equation of Table VII. The angular scale corresponds to the experimental coordinate ψ as shown in Fig. 7.

TABLE VI. Cyclotron effective masses for the α orbit on the open-hole sheet of the Fermi surface of Pd.

Plane	ψ	θ	φ	Expt m^*	Calc[a] m^*
e	40	21.75	−75.34	2.613	2.705
f	24	29.90	−112.99	3.157	3.083
	29	24.72	−113.68	2.855	2.805
	34	19.55	−114.74	2.666	2.630
	39	14.40	−116.53	2.553	2.519
	43	10.29	−119.25	2.421	2.463
	45.5	7.74	−122.40	2.437	2.437
	48	5.24	−128.59	2.379	2.420
	50.5	2.91	−145.24	2.429	2.410
	53	1.70	152.67	2.423	2.407
	140	19.14	1.38	2.677	2.643
	142.5	19.41	9.19	2.627	2.646
	145	20.00	16.68	2.704	2.655
	148	21.09	24.99	2.668	2.673
	154	24.30	38.88	2.831	2.792
	157	26.28	44.49	2.898	2.926
	160	28.46	49.34	3.082	3.138
g	0	154.25	175.84	2.869	2.813
	4	157.06	−176.73	2.736	2.745
	8	159.43	−167.53	2.682	2.647
	12	161.20	−156.37	2.608	2.612
	15	162.03	−146.86	2.573	2.582
	18	162.36	−136.73	2.541	2.569
	171	27.62	−8.44	2.772	2.855

[a]Using the expansion coefficients of Table VII.

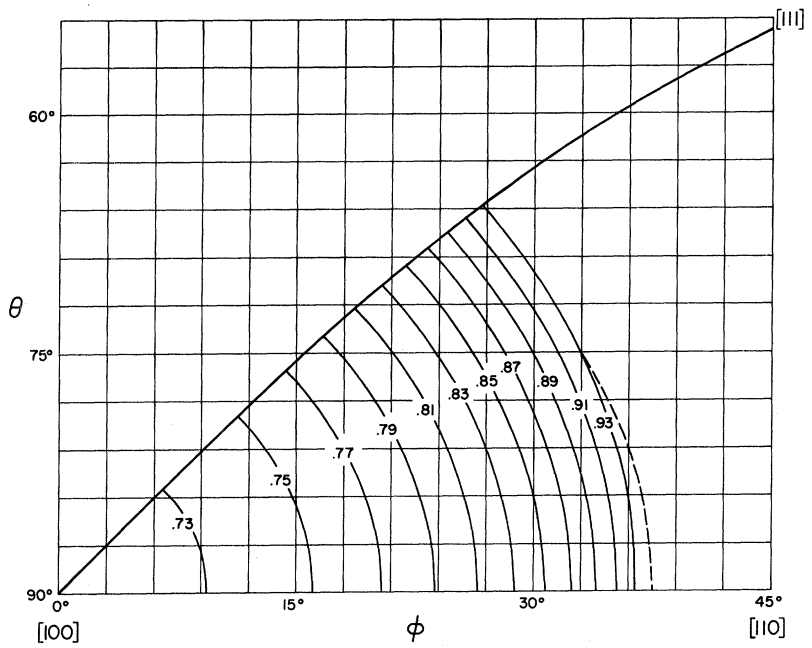

FIG. 17. Contours of constant area for the α orbit on the open-hole sheet of the Fermi surface of Pd in the basic triangle. The dashed line shows the boundary beyond which the orbit ceases to exist.

We have observed the effects of exchange splitting in two palladium alloys, one having 0.10 at.% cobalt and the second 0.05 at.% cobalt.[42] With the field along the [100] direction of the crystal we were able to observe beats in the dHvA oscillations arising from the small area cross section of the X-centered pockets. From the observed beat frequency we calculate the area shifts $\Delta A(0.05\%) = 1.40\times10^{-4}$ and $\Delta A(0.10\%) = 2.87\times10^{-4}$ a.u. The resulting energy shifts are $\Delta E(0.05\%) = 1.09\times10^{-4}$ and $\Delta E\ (0.10\%) = 2.23\times10^{-4}$ Ry, where we have used the unenhanced band mass of 0.41.[10] If this exchange splitting were constant over the surface and, moreover, the same for all sheets of the surface, the total band contribution to the magnetization, m_s^{band}, would be given by

$$m_s^{\text{band}} = \tfrac{1}{2}\mu_B N(E_F)\,\Delta E^{ex}\ .$$

Using the value $N(E_F) = 32$ states/atom Ry, this gives $m_s^{\text{band}}\ (0.05\%) = 1.09$ and $m_s^{\text{band}}\ (0.10\%) = 2.24$

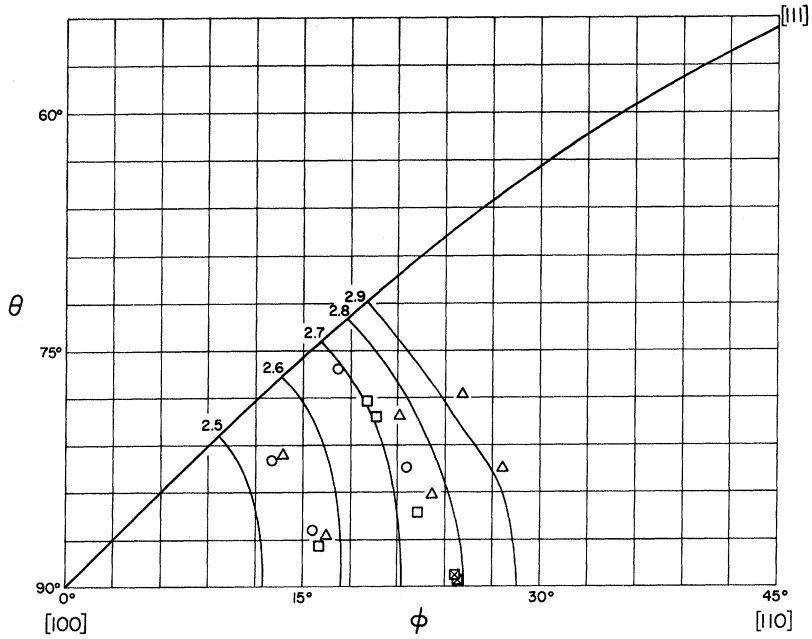

FIG. 18. Contours of constant cyclotron effective mass for the α orbit on the open-hole sheet of the Fermi surface of Pd in the basic triangle. Shown also are the angles at which spin-splitting zeros were observed.

TABLE VII. Area and cyclotron effective mass expansion coefficients for the α orbit on the open-hole sheet of the Fermi surface of Pd.

$\frac{1}{A^2(\theta,\varphi)} = \sum_{l,m} \alpha_{l,m} C_{l,m}(\theta,\varphi)$		$\frac{1}{m^{*2}(\theta,\varphi)} = \sum_{l,m} \alpha'_{l,m} C_{l,m}(\theta,\varphi)$	
$\alpha_{0,0}$	69.064	$\alpha'_{0,0}$	−0.5295
$\alpha_{2,0}$	303.103	$\alpha'_{2,0}$	0.6784
$\alpha_{4,0}$	−20.219	$\alpha'_{4,0}$	−0.1553
$\alpha_{4,4}$	−98.528	$\alpha'_{4,4}$	4.0921
$\alpha_{6,0}$	− 0.811	$\alpha'_{6,0}$	0.0253
$\alpha_{6,4}$	2.561	$\alpha'_{6,4}$	−0.6187

emu/cm^3. These values are much smaller than the values m_s^{band} (0.05%) = 2.2 and m_s^{band} (0.10%) = 4.4 emu/cm^3 which correspond to a band contribution to the moment of 7 μ_B per cobalt atom (9 μ_B, the observed saturation magnetization, less 2 μ_B the cobalt atomic moment). We believe this discrepancy to arise primarily from an exchange splitting which is different for each sheet of the Fermi surface, largest for the heavy-hole sheet, and which varies over each sheet. Inaccuracies in the extrapolated value of 9 μ_B for the value of μ_{eff} in dilute alloys of Co in Pd[1] or in the assumed moment of 2 μ_B for the cobalt atom must be much too small to account for the above discrepancy.

The assumption that the exchange splitting ΔE^{ex} varies from sheet to sheet of the Fermi surface is supported by the alloy dHvA data from the Γ-centered electron surface. Oscillations arising from this surface were observed only over the limited magnetic-field range from about 55–72 kG, this latter field being the limit of the magnetic field available with our superconducting solenoid. With this field range we were not able to resolve any beat waists, although several field orientations showed a small reduction of the dHvA amplitude with increasing field. This indicates the onset of a beat null which would occur somewhat above our maximum available field. From the field range over which no beats were observed we can set an upper limit to the exchange splitting using an unenhanced cyclotron effective mass for the Γ-centered electron surface. Such estimates show that the exchange splitting for this surface must be substantially less than 1.5×10^{-4} and 1.8×10^{-4} Ry for the 0.05% and 0.10% alloys, respectively. Comparison with the exchange splitting on the ellipsoid sheet shows that, at least for the 0.10% alloy, the value for the Γ-centered sheet is considerably less than for the ellipsoid sheet. Because of the high cyclotron effective masses associated with the open-hole sheet of the Fermi surface, no dHvA oscillations arising from this sheet were observed in the alloys and no estimate of the corresponding exchange splitting could be made.

Further evidence for the existence of the exchange splitting was found in the examination of the dHvA field-rotation patterns corresponding to the Γ-centered electron sheet. When the field was rotated through orientations where spin-splitting zeros occurred in the pure material, sharp nulls were observed in the field-rotation patterns. When the same field rotations were performed in the alloys, no nulls were observed in the field-rotation patterns. Such behavior clearly demonstrates the disappearance of the spin-splitting-zero phenomenon as would be expected for exchange split bands.

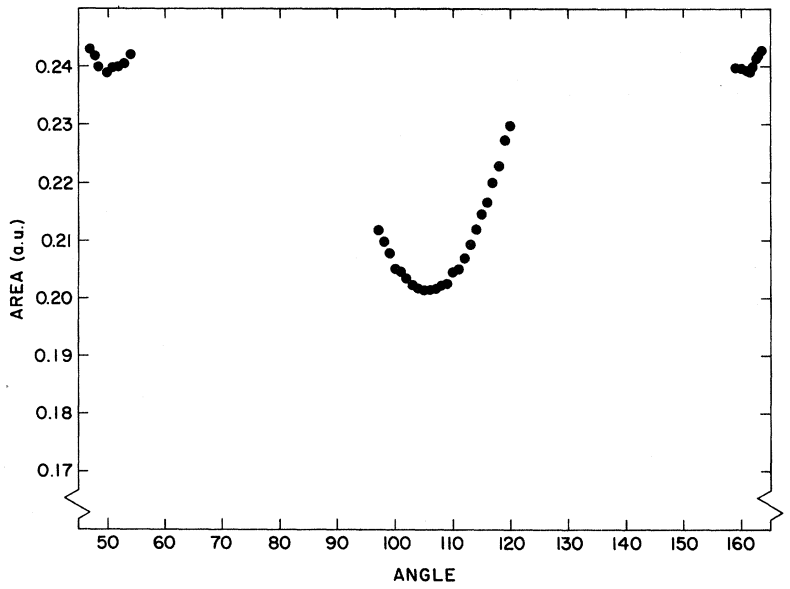

FIG. 19. Angular dependence of the extremal areas for the γ orbit on the open-hole sheet of the Fermi surface of Pd observed in plane g. The angular scale corresponds to the experimental coordinate Ψ as shown in Fig. 7.

Further discussion and illustrations of the relevant data can be found in Ref. 42.

VII. CONCLUSIONS

When the rather extensive data collected here are analyzed, several important conclusions can be drawn. Perhaps most striking of these is found in the comparison of this work with our earlier work in Pt. The similarity of the Fermi surface in these two isoelectronic materials is much more complete than expected. Surprising, however, is the fact that although the shapes of the surfaces in the two materials are almost identical, the underlying band structures seem to be quite different, at least with respect to the behavior of the bands near the Fermi level. This is evidenced quite clearly in the very different behavior in the two materials of the cyclotron effective mass and Fermi velocity on the Γ-centered electron sheets. In Pd, as in Pt, the agreement between the experimental Fermi surface and the band-structure calculations is very good. Further, the qualitative difference between Pt and Pd in the behavior of the cyclotron effective masses and Fermi velocities is also predicted by the band-structure calculations. With the encouragement of such successes in the calculation of band structures it is hoped that further work will be attempted, both in the improvement of the accuracy of the present calculations and in the formulation of techniques to calculate the less understood aspects of the experimental data presented here. Two important problems lie in the explanation of the g-factor data (both from a single-particle and many-particle point of view) and in the calculation of the many-body alteration of the cyclotron effective mass and Fermi velocity.

ACKNOWLEDGMENTS

We would like to thank O. K. Andersen, A. R. Mackintosh, and F. M. Mueller for making available the results of their band-structure calculations before publication.

---

*Work performed under the auspices of the U. S. Atomic Energy Commission.

†Present Address: Department of Physics, Uppsala University, Uppsala, Sweden.

[1]R. M. Bozorth, P. W. Wolff, D. D. Davis, V. B. Compton, and J. H. Wernick, Phys. Rev. 122, 1157 (1961).

[2]J. Crangle and W. R. Scott, J. Appl. Phys. 36, 921 (1965).

[3]F. E. Hoare and J. C. Matthews, Proc. Roy. Soc. (London) A212, 137 (1952); J. Wucher, Compt. Rend. 242, 1143 (1956).

[4]E. C. Stoner, Proc. Roy. Soc. (London) A165, 372 (1938).

[5]S. Doniach, in Proceedings of the Manchester Many Body Conference, 1964 (unpublished).

[6]N. F. Berk and J. R. Schrieffer, Phys. Rev. Letters 17, 433 (1966).

[7]S. Doniach and S. Engelsberg, Phys. Rev. Letters 17, 750 (1966).

[8]F. E. Hoare and B. Yates, Proc. Roy. Soc. (London) A240, 42 (1957).

[9]A. J. Freeman, J. O. Dimmock, and A. M. Furdyna, J. Appl. Phys. 37, 1256 (1966).

[10]O. K. Andersen and A. R. Mackintosh, Solid State Commun. 6, 285 (1968).

[11]O. K. Andersen, Phys. Rev. B 2, 1883 (1970).

[12]F. M. Mueller, A. J. Freeman, J. O. Dimmock, and A. M. Furdyna, Phys. Rev. B 1, 4617 (1970).

[13]J. B. Ketterson and L. R. Windmiller, Phys. Rev. B 2, 4813 (1970).

[14]See, for example, *Methods in Computational Physics*, Vol. 8, edited by B. Alder, S. Fernbach, and M. Rotenberg; *Energy Bands of Solids* (Academic, New York, 1969).

[15]Y. Onodera and M. Okazaki, J. Phys. Soc. Japan 21, 1273 (1966).

[16]See, for example, T. L. Loucks, *Augmented Plane Wave Method* (Benjamin, New York, 1967).

[17]F. M. Mueller, Phys. Rev. 153, 659 (1967).

[18]J. Friedel, P. Lenglart, G. Leman, J. Phys. Chem. Solids 25, 781 (1964).

[19]I. M. Lifshitz and A. M. Kosevich, Zh, Eksperim. i Teor. Fiz. 29, 730 (1955) [Sov. Phys. JETP 2, 636 (1956)].

[20]L. Onsager, Phil. Mag. 43, 1006 (1952).

[21]I. M. Lifshitz and A. V. Pogorelov, Dokl. Akad. Nauk. SSSR 96, 1143 (1954).

[22]F. M. Mueller, Phys. Rev. 148, 636 (1966).

[23]F. M. Mueller and M. G. Priestley, Phys. Rev. 148, 638 (1966).

[24]L. L. Foldy, Phys. Rev. 170, 670 (1968).

[25]J. B. Ketterson, L. R. Windmiller, S. Hörnfeldt, and F. M. Mueller, Solid State Commun. 6, 851 (1968).

[26]J. B. Ketterson and L. R. Windmiller, Phys. Rev. B 1, 463 (1970).

[27]R. Aurbach, J. B. Ketterson, and L. R. Windmiller, J. Phys. Chem. Solids (to be published).

[28]R. Aurbach, J. B. Ketterson, F. M. Mueller, and L. R. Windmiller, ANL Report No. 7659 (unpublished).

[29]D. J. Roaf, Phil. Trans. Roy. Soc. (London) A255, 135 (1962).

[30]J. B. Ketterson, F. M. Mueller, and L. R. Windmiller, Phys. Rev. 186, 656 (1969).

[31]S. Hörnfeldt, J. B. Ketterson, and L. R. Windmiller, in Proceedings of the NBS Density of States Conference, 1969 (unpublished).

[32]B. Bosacchi, J. B. Ketterson, and L. R. Windmiller, Phys. Rev. B 2, 3025 (1970).

[33]B. Bosacchi, J. B. Ketterson, and L. R. Windmiller (to be published).

[34]M. R. Halse, Phil. Trans. Roy. Soc. London 265, 507 (1969).

[35]F. M. Mueller, L. R. Windmiller, and J. B. Ketterson, J. Appl. Phys. 41, 2312 (1970).

[36]R. W. Stark and L. R. Windmiller, Cryogenics 8, 272 (1968).

[37]L. R. Windmiller and J. B. Ketterson, Rev. Sci. Instr. 39, 1672 (1968).

[38]Johnson Matthey Chemicals Limited, 74 Hatton Garden, London, E. C. 1, England.

[39]J. B. Ketterson, J. S. Tait, and L. R. Windmiller, J. Crystal Growth 1, 323 (1967).

[40]S. Hörnfeldt, J. B. Ketterson, and L. R. Windmiller, J. Crystal Growth 5, 289 (1969).

[41]H. F. Sterling and R. W. Warren, Metallurgia 67, 1 (1963).

[42]S. Hörnfeldt, J. B. Ketterson, and L. R. Windmiller, Phys. Rev. Letters 23, 1292 (1969).

[43]L. R. Windmiller and J. B. Ketterson, Phys. Rev. Letters 21, 1076 (1968).

[44]The heavy solid-line contour of Fig. 14(b) was chosen as shown because of the similarity to the contour in platinum. However, with the available data a second possibility for the connectivity of the contours exists. The contour crossing the (110) plane at approximately $\theta = 73°$, $\varphi = 17°$ could follow the course shown up to $\varphi = 35°$, where it could turn and cross the (100) plane around $\varphi = 37°$. Then the remainder of the contour crossing the (110) plane at $\theta = 88°$ would be free to turn back and join the dotted contour at $\theta = 86°$ forming a contour much like the 2.35 cyclotron effective-mass contour.

[45]S. Engelsberg and G. Simpson, Phys. Rev. B 2, 1657 (1970).

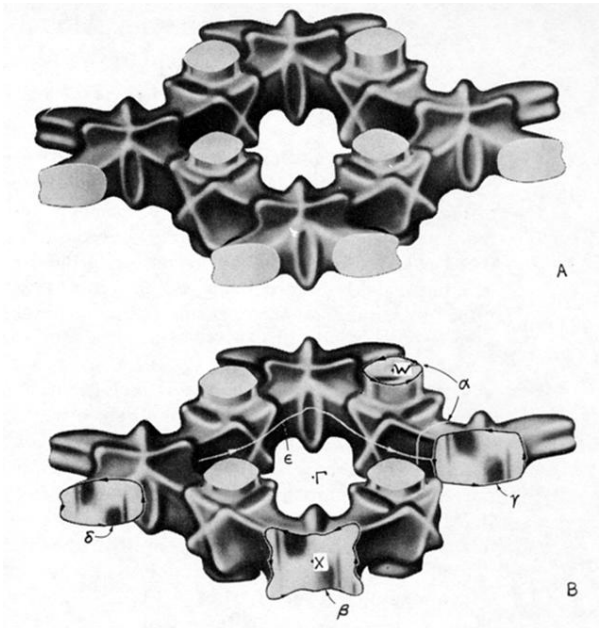

FIG. 3. (a) Open-hole sheet of the Fermi surface of Pd showing connectivity, viewed from approximately the ⟨111⟩ direction. (b) Cutaway of the open-hole sheet of the Fermi surface of Pd showing the various expected extremal orbits.

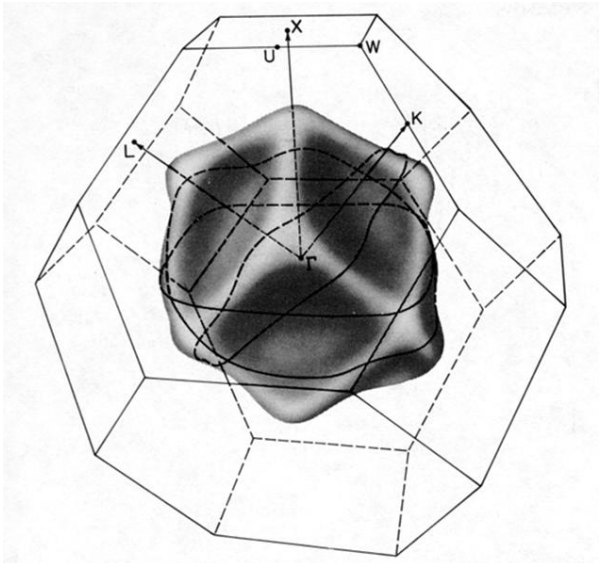

FIG. 4. The Γ-centered electron sheet of the Fermi surface of Pd. Shown are the extremal DHvA orbits for the magnetic field parallel to ⟨100⟩, ⟨110⟩, and ⟨111⟩.

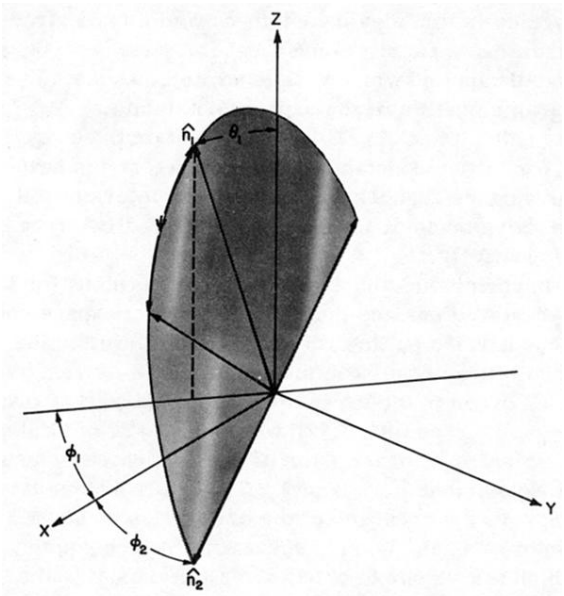

FIG. 6. Plane of rotation of the sample as specified by the vectors $\hat{n}_1$ and $\hat{n}_2$ (see text).